SAND2013-10312C

Terahertz near-field probe incorporating a λ/100 aperture for time-domain spectroscopy and imaging

Alexander J. Macfaden[a], John L Reno[b,c], Igal Brener[b,c], Oleg Mitrofanov[a,b] *

[a] Department of Electronic & Electrical Engineering, UCL, London, WC1E 7JE, UK
[b]Center for Integrated Nanotechnologies, Sandia National Laboratories, NM 87185, USA
[c]Sandia National Laboratories, NM 87185, USA
*o.mitrofanov@ucl.ac.uk

ABSTRACT

Achieving high spatial resolutions for imaging with terahertz (THz) waves requires near-field probes, such a as a sub-wavelength aperture probe. Bethe's theory of transmission through a sub-wavelength aperture of size a predicts that that transmitted electric field scales as $E \propto a^3$. This strong dependence limits the size of apertures that can be employed and hence the spatial resolution. This dependence however changes for the evanescent field components in a very close proximity (~1μm for THz waves) to the aperture, as shown by electromagnetic simulations. To exploit this effect in a THz near-field probe, we developed a photoconductive THz near-field detector structure, which incorporates a thinned photo-conductive detector region and a distributed Bragg reflector between the detector and the aperture plane. Near-field probes are manufactured with different aperture sizes to investigate transmission of THz pulses through apertures as small as 3μm. The experimental results confirm that the transmitted field amplitude, and therefore the sensitivity, increases by about one order of magnitude for the new probes. The 3μm aperture probe with the spatial resolution of λ/100 at 1THz is demonstrated.

Keywords: terahertz, near-field, time-domain spectroscopy, photonic nanostructure, FDTD

1. INTRODUCTION

Spatial resolution beyond the diffraction limit in Terahertz (THz) imaging is achieved using near-field scanning probes.[1-8] Sub-wavelength aperture probes and electro-optic probes so far have reached a spatial resolution of ~7-10μm,[2-5] whereas scattering needle probes in AFM or STM systems showed a spatial resolution better than 1μm.[6,7] The electro-optic and aperture probes however produce THz images, which typically correlate with the electric field distribution near the sample surface illuminated by a THz beam, showing the interaction of the THz wave with the sample directly, while the scattering probes tend to show the sample interaction with the probe. Each THz microscopy application therefore determines an appropriate probe type. Limits of spatial resolution achievable with an aperture probe are explored here.

The limited spatial resolution with the sub-wavelength aperture probe is attributed to the transmission properties of single sub-wavelength apertures. According to Bethe's theory, the transmitted field amplitude (E) follows an a^3 power dependence (i.e. intensity $I \sim a^6$) for apertures $a \ll \lambda$.[9-11] We have demonstrated recently that the prohibitive Bethe dependence can be overcome by placing the THz detector within ~1μm from the aperture.[12] The detector in this case senses the evanescent field components that do not follow the a^3 power dependence.[1,13]

Here we discuss the design required to capitalize on the evanescent field enhancement very close (within ~1μm) to the aperture, both in simulation and experimentally. To take advantage of the evanescent field for small apertures, the entire THz detector must be sufficiently small to be accommodated within a short range (~1μm) of the aperture. This is accomplished by creating a photonic nanostructure. Using such a probe, we present the highest spatial resolution (3μm) achieved to date with an aperture-type near-field probe for THz time-domain spectroscopy and imaging.[1] Further details of this work can be found in Ref. 12.

2. PHOTONIC NANOSTRUCTURE

The structure of the device is shown in Fig. 1(a). A distributed Bragg reflector (DBR) is situated between the photo-conductive detector region and the aperture plane. The DBR has two main purposes. Firstly, the photoconductive layer behaves like a low-Q cavity, leading to enhanced optical fields and increased carrier generation efficiency. Secondly, optical isolation prevents the gating optical pulse passing through the near-field probe and reaching the sample. The latter is required for imaging applications, as it permits imaging of light sensitive samples, such as semiconductor-based metamaterials, and reduces the effect of false contrast that can arise if the sample has non-uniform optical reflectivity.

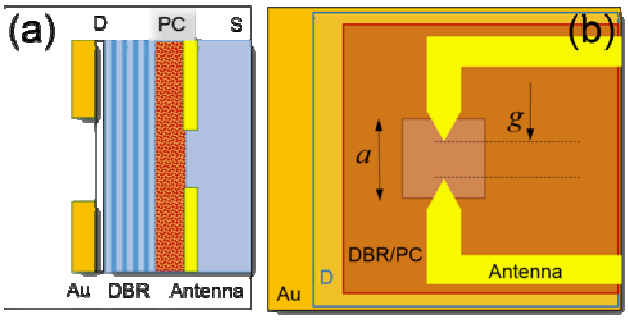

FIG. 1: Schematic cross-section (a) and diagram (b) of the integrated THz near-field probe: Au – gold screen with an aperture, D – insulating dielectric layer; DBR – distributed Bragg reflector, PC – photoconductive LT GaAs layer, S – sapphire substrate.

The structure is grown by MBE and it consists of a 505nm thick, low-temperature grown (LT) GaAs active region, chosen as a multiple of λ/4 of the gating pulse wavelength (800nm). The DBR is made up of 9 λ/4 layers of AlAs and $Al_{20\%}Ga_{80\%}As$. The DBR is separated from the metallic screen by a dielectric spacer layer made of either a combination of the 527 nm thick $Al_{20\%}Ga_{80\%}As$ layer and a 68nm AlAs layer (both in multiples of λ/4), or by a 30nm thick Al_2O_3 film. The distance from the aperture plane to the detector antenna is therefore ~1.6μm and 1.0μm respectively in these two designs. A set of THz near-field probes is fabricated following the process described in Ref. 2. The THz detector antenna is aligned with the aperture as shown in Fig. 1(b).

The combination of the DBR, the LT-GaAs layer and the spacer layer minimizes optical transmission of the optical gating pulse at the excitation wavelength. The optical transmission spectrum for the 1.6μm-thick hetero-structure (mounted on a sapphire substrate and normalized to the substrate transmission coefficient) has a minimum of <10% near the excitation wavelength (800 nm). Periodic variation of the transmission coefficient shows the DBR effect (Fig. 2).

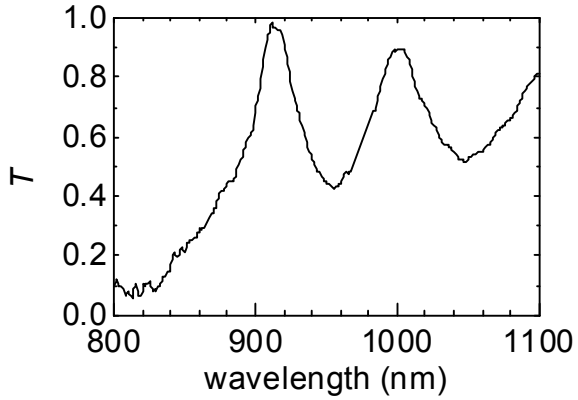

FIG 2: The optical transmission spectrum of the probe hetero-structure (without the gold screen) normalized to the transmission through the sapphire substrate.

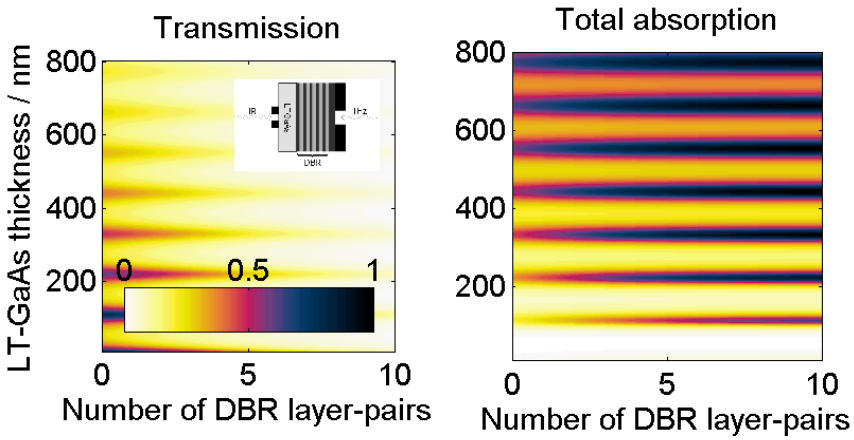

FIG. 3: The transmission and total absorption (arb. units) for given LT-GaAs photodetective layer thickness and number of DBR layer pairs as shown in the inset. The Fabry-Pérot resonances are clear as the horizontal features.

There is further scope for optimization of the photonic structure of the device. The current design has been optimized to minimize the transmission at the gating pulse wavelength (800nm). However, the optical transmission is not the only critical metric. The probe sensitivity is essential and it is affected by the design of the photonic structure.

The sensitivity depends on the photo-generated carrier density, and hence the optical field intensity, which can be increased by making the LT-GaAs layer into an optical cavity. Intensity is significantly enhanced around the Fabry-Pérot resonances, but at the expense of increased transmission, as shown in Fig 3. For thinner devices, the conflict between reducing transmission and improving absorption is most striking. The optimum design depends on the sensitivity requirements, but in general the best configuration is to have the LT-GaAs layer near to, but not on, a resonance. This demonstrates the further scope for optimizing the device structure by adjusting the epilayer design.

3. NEAR-FIELD PROBE SENSITIVITY

We evaluate the THz probe sensitivity experimentally by comparing the amplitude and waveforms of detected THz pulses using near-field probes with different designs. The experimental setup is shown schematically in Fig. 4. The THz pulses are generated by optical rectification in a ZnTe crystal, and delivered to the sample by a 1mm diameter waveguide, which ensures unfocussed THz illumination.[14] The optical gating pulses (mode-locked Ti:Sapphire laser, τ = 100fs, λ= 800nm) are focused on the antenna gap using a lens (NA=0.5).

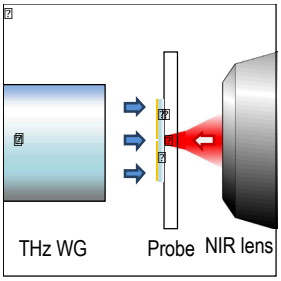

FIG. 4: The experimental setup for measuring probe sensitivity. Unfocussed THz radiation from the waveguide illuminates the probe from one side; the photocarrier generating pulse is incident from the other side.

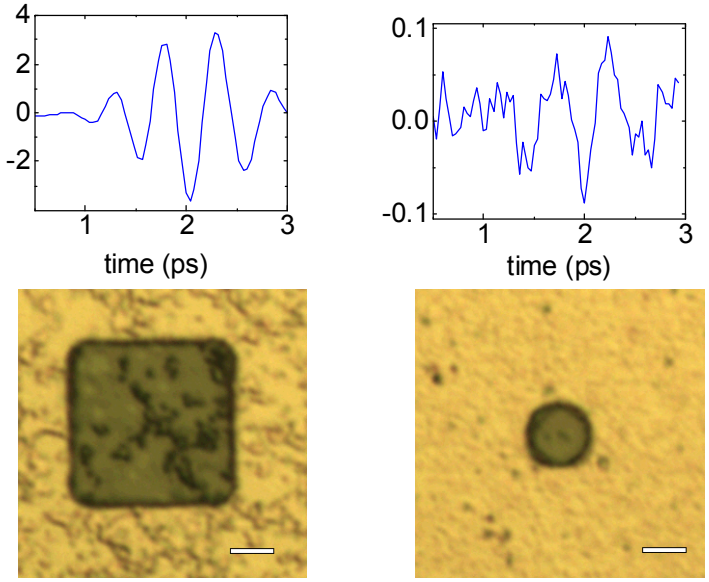

FIG. 5: Waveforms from the 10μm (*left*) and 3μm (*right)* apertures. The detector-aperture separation is 1.6μm, and the antenna gap is 7.5μm. Microscope images of the apertures are shown below *(scalebar = 3μm)*.

A comparison of the THz pulse waveforms transmitted through a 10μm and 3μm apertures is shown in Fig. 5. The 3μm aperture signal is significantly weaker, but it has the same waveform. The pulse waveform remains unchanged for all tested probes, agreeing with the findings that the waveform of the transmitted THz pulse is independent of the aperture size in the regime $a < \lambda/10$ and that the waveform corresponds to a temporal derivative of the incident wave.[15] The fact that the waveforms are the same allows us to compare the signal strength in both the temporal and spectral domains.

Fig. 6 shows the normalized signal amplitudes for a range of probes of different configurations (see full discussion in Ref. 12). The amplitude of the detected THz field decreases rapidly as the aperture size decreases. It follows the a^3 dependence for relatively large aperture-antenna separations (4μm), but relaxes to a weaker dependence for the 1.6 to 1μm separations.

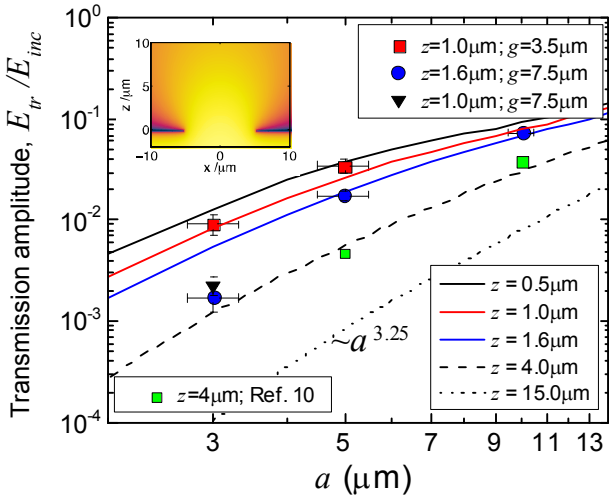

FIG. 6: Transmitted THz field amplitude (*reproduced from Ref. 12*). Symbols show the measurements at a distance of z = 1μm and 1.6μm from the aperture, and lines show numerical calculations. Green symbols show the transmitted amplitude data for z = 4μm.[11] The inset: the electric field intensity $\langle E_x^2 \rangle$ in the near-field of a 10μm aperture.

The effect of reducing the aperture-detector separation is clear: the 5μm aperture probes with the 1μm aperture-antenna separation show approximately one order of magnitude higher signal compared to the separation of 4μm. This effect becomes even stronger for smaller apertures.

To analyze the functional dependence of the amplitude on aperture size, we compare the experimental results to the numerically computed amplitude of the electric field within a short distance of the apertures. The finite-difference time-domain method[16] is used to model THz pulse transmission through square holes in a 300nm thick gold film placed on a GaAs substrate. The transmitted amplitude is calculated for the spectral range 1–1.5THz and normalized to the amplitude of the incident field to match the experimental conditions used in this work, as well as in a previous study of aperture transmission for comparison.

In Fig. 6, the simulation results clearly show the benefits of moving the detector antenna close to the aperture. For z = 15μm, a dependence of slightly worse than a^3 is found. The extra losses beyond the Bethe model are associated with the finite thickness of the metallic screen, which introduces waveguiding losses, and the Ohmic losses. We note that the a^3 dependence persists for z significantly smaller than the wavelength (for the evanescent components). The power law however changes gradually towards a linear dependence $E \sim a^1$, found for z = 0 in the plane of the aperture.[1,13] The amplitude of the transmitted field increases significantly.

The functional dependences calculated for z = 1.0μm and for z = 1.6μm are followed by the experimental results closely except for the 3μm probes with g=7.5μm, for which the detected signal is noticeably weaker than predicted by calculations. This is attributed to the antenna tips being spaced further apart than the aperture size, meaning that the average field between the tips is reduced by approximately a factor of 2-3, consistent with the measured amplitude. This observation highlights the importance of scaling the photoconductive antenna gap with the aperture size in order to take advantage of the evanescent field, which is present only in the area of the aperture.

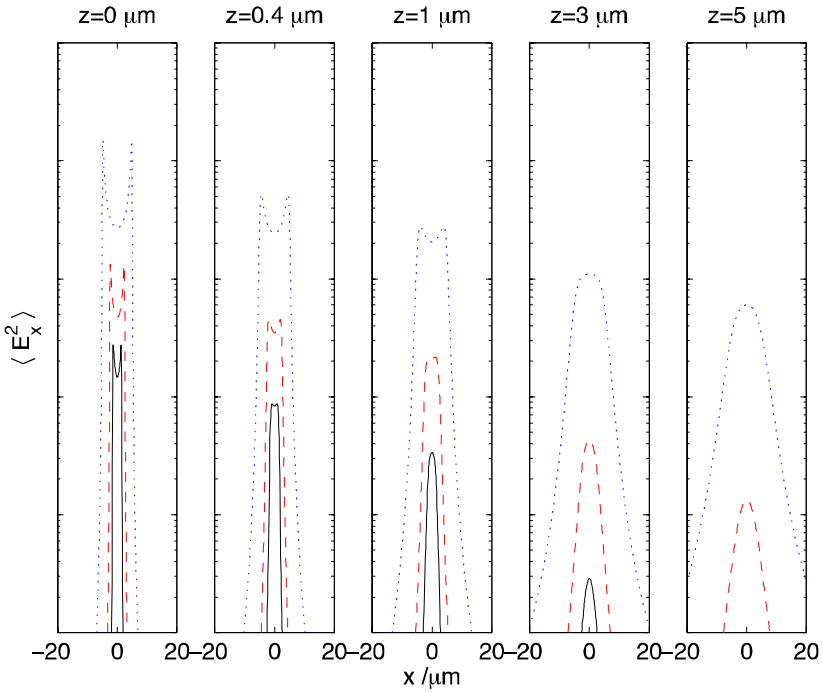

FIG. 7: Cross sections of the field across the aperture, $\langle E_x^2 \rangle$, at different heights z above the aperture. The black solid lines is a 3μm aperture; red dashed is 5μm; and blue dotted is 10μm.

Fig. 7 demonstrates this effect by showing the form of the electric field profile at different distances from the aperture as calculated by the FDTD software for different apertures. The field drops off very quickly at the edge of the aperture, demonstrating the requirement that the antenna gap be modified to equal to or less than the size of the aperture. Very close to the aperture the E_x field component has a local minimum in the center of the aperture, with stronger electric field

found above the edges of the aperture. These evanescent components correspond to high k–vector in the angular spectrum representation $E(\omega, k_x, k_y)$ and decay very quickly. They are due to the dipole-like field radiated by the surface charges required to satisfy the boundary conditions on the aperture edge.

4. SPATIAL RESOLUTION OF THE APERTURE PROBE

Spatial resolution capabilities of the integrated near-field probes are evaluated by scanning an edge of a metallic strip deposited on GaAs in front of the 3μm aperture probe. For this experiment we used an unfocused THz beam generated using the ZnTe crystal positioned approximately 5mm away from the test sample. The metallic edge is oriented parallel to the beam polarization. The THz pulse waveform is shown in Fig. 8(a). The amplitude of the THz pulse changes between the metallic and dielectric regions (Fig. 8(b), red line) with the transition region length of 3.3±0.5μm using the 10-90% criterion or 2.5μm using the 20-80% criterion. This test confirms that the probe spatial resolution is determined by the aperture size.

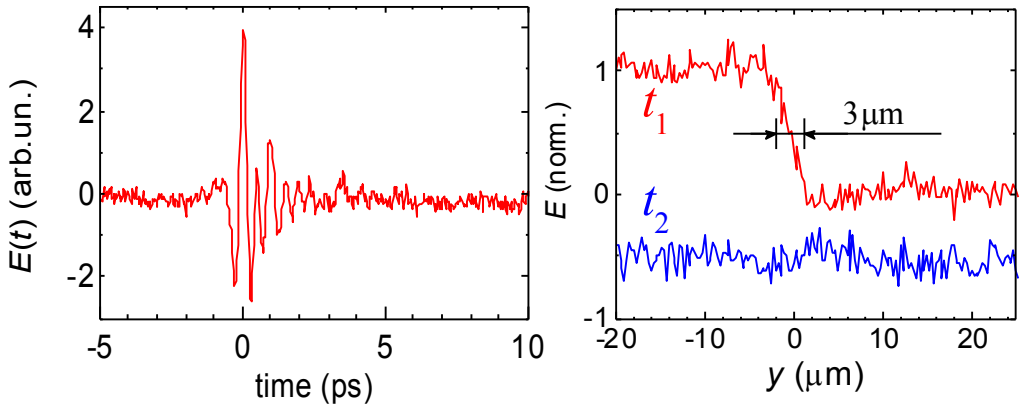

FIG. 8: (a) THz pulse waveform detected by a 3μm aperture probe (z=1.0μm, g=3.5μm). (b) Normalized traces of the field amplitude detected by the probe when a metallic edge is scanned over the aperture: t_1 represents the detected field amplitude at the peak of the pulse (t=0) and t_2 represents the field 2ps prior the pulse arrival The t_2 trace is offset by -0.5 for clarity (*Reproduced from Ref. 12*).

5. CONCLUSIONS

In conclusion, integrated photo-conductive THz near-field probes are manufactured with different aperture sizes to investigate transmission of THz pulses through apertures as small as 3μm. The experimental results confirm that the transmitted field amplitude, and therefore the sensitivity, increases by about one order of magnitude for the new probes. The signal strength dependence on the aperture size and the distance from the aperture agrees well with FDTD simulations. The 3μm aperture probe is shown to provide a spatial resolution of λ/100 at 1THz. The results suggest that further improvements in resolution for the aperture-type THz near-field probes are possible by optimizing both the probe photonic nanostructure and the detector antenna design.

6. ACKNOWLEDGEMENTS

We would like to thank Prof. Paul Planken for useful discussions of wave transmission through small apertures and gratefully acknowledge the support of the Royal Society [Grant No. UF080745]. This work was performed, in part, at the Center for Integrated Nanotechnologies, an Office of Science User Facility operated for the U.S. Department of Energy (DOE) Office of Science. Sandia National Laboratories is a multi-program laboratory managed and operated by Sandia Corporation, a wholly owned subsidiary of Lockheed Martin Corporation, for the U.S. Department of Energy's National Nuclear Security Administration under contract DE-AC04-94AL85000.

REFERENCES

[1] A. J. L. Adam, J Infrared Millimeter Terahertz Waves 32, 976 (2011).
[2] O. Mitrofanov, M. Lee, J. W. P. Hsu, I. Brener, R. Harel, J. Federici, J. D. Wynn, L. N. Pfeiffer, and K. W. West, IEEE J. Selected Topics in Quantum Electronics 7, 600 (2001).
[3] F. Blanchard et al., Annu. Rev. Mater. Res. 43, 237 (2013).
[4] Y. Kawano et al., Nature Photonics 2, 618 (2008).
[5] A. J. L Adam, N. C. J. van der Valk, P. C. M. Planken, J. Opt. Soc. A. B 24, 1080 (2007)
[6] K. Moon et al., Appl. Phys. Lett. 101, 011109 (2012).
[7] T. L. Cocker et al., Nature Photonics 7, 620 (2013).
[8] M. Wachter, M. Nagel, and H. Kurz, Appl. Phys. Lett. 95, (2009)
[9] H. Bethe, Physical Review **66**, 163 (1944).
[10] C. J. Bouwkamp, Philips Res. Rep **5** (1950).
[11] O. Mitrofanov, M. Lee, J. W. P. Hsu, L. N. Pfeifer, K. W. West, J. D. Wynn, and J. F. Federici, Appl. Phys. Lett. **79**, 907 (2001).
[12] A. Macfaden, J. Reno, I. Brener, and O. Mitrofanov, '3μm aperture probes for near-field terahertz transmission microscopy,' Appl. Phys. Lett. *submitted for publication*
[13] J. R. Knab, A. J. L. Adam, E. Shaner, H. J. A. J Starmans, P. C. M. Planken, Optics Express **21**, 1, 1101 (2013).
[14] M. Navarro-Cia, M. S. Vitiello, C. M. Bledt, J. E. Melzer, J. A. Harrington, and O. Mitrofanov, Optics Express 21, 23748 (2013).
[15] O. Mitrofanov, L. N. Pfeiffer, and K. W. West, Appl. Phys. Lett. **81,** 1579 (2002).
[16] Lumerical Solutions Inc, *Lumerical FDTD Solutions*, URL http://www.lumerical.com/tcad-products/fdtd/.